Research Article

Chao Kong, Bin Yin, Jiaxin Wu, Jianquan Huang, Dajun Lei, Chunzhi Jiang, and Haiming Deng*

Stability control in a helicoidal spin–orbit-coupled open Bose–Bose mixture

https://doi.org/10.1515/phys-2022-0263
received January 03, 2023; accepted June 09, 2023

Abstract: In this article, the modulation instability (MI) of open Bose–Bose mixtures with helicoidal spin–orbit coupling (SOC) was studied. Unlike previous spin–orbit (SO)-coupled Bose–Einstein condensate system with helicoidal gauge potential, the purpose of this article to study the input of the helicoidal SOC in the emergence of MI in open Bose–Bose mixtures by taking into account the Lee–Huang–Yang corrections to the coupled Gross–Pitaevskii equations. We present the detailed analyses of system parameters on the characteristics of MI and analytically conclude the parameter conditions for MI occurrence. Our results provide a potential way to manipulate the MI in the helicoidal SO-coupled open Bose–Bose mixtures.

Keywords: modulation instability, Bose–Bose mixtures, spin–orbit coupling, stability analysis, open system

1 Introduction

As a fundamental ingredient of the matter–wave dynamics, the modulation instability (MI) is a result of the constructive interplay between dispersion and nonlinearity and has been addressed in dispersive nonlinear systems, such as in the optical fiber [1], in electrical transmission lines [2,3], in metamaterials [4], and in biophysical systems [5–7]. Moreover, MI in the single-component Bose–Einstein condensate (BEC) with attractive atomic interaction and two-component BEC even with repulsive interaction has been shown [8–11]. Clearly, MI is the key mechanism for the formation of soliton trains in BEC [12].

The dynamics and stability of quantum droplets have been presented [13–15]. For example, for a Bose–Bose mixture with repulsive intra- and attractive interspecies interactions, the quantum Lee–Huang–Yang (LHY) repulsion neutralizes the mean field attraction and stabilizes the system against collapse [13]. In one-dimensional (1D) weakly interacting Bose–Bose mixtures, the beyond mean field attractive energy stabilizes a repulsive mean field term [14]. Moreover, spin–orbit coupling (SOC) can also stabilize quantum droplets. SOC, the interaction between the spin and momentum of a quantum particle, accounts for many condensation phenomena as diverse as spin Hall effect [16,17], topological insulators [18,19], and so on. Recently, the 1D SOC has been realized in cold-atom system [20], and the very recent works have revealed the tunability of SOC strength by the magnitude and direction of the Raman laser wave-vector [21]. Inspired by that, many activities have been taken to understand the dynamics of a spin–orbit (SO)-coupled BEC [22–30]. MI in 1D and two-dimensional SO-coupled BEC has been recently investigated [31–34]. In particular, the dynamical behavior of MI in helicoidal SO-coupled BEC is addressed [35], and the helicoidal gauge potential can arise in description of light propagation in helical waveguide arrays [36]. On the other hand, the MI growth rate of Bose–Bose mixture in the presence of SO and Rabi couplings shows distinct signatures of the couplings, in the form of multiple domains of instability [37]. Generation of matter waves in Bose–Bose mixtures with helicoidal SOC is addressed [38], and they present that symmetry-breaking perturbations appear for suitably chosen system and wave parameters, which manifest themselves through the emergence of trains of quantum droplets. Inspired by these achievements, we are curious what are the characteristics of the MI in helicoidal SO-coupled open Bose–Bose mixtures, which remains an open problem.

In this article, we consider the helicoidal SO-coupled open Bose–Bose mixtures through which we study the MI. We restrict ourselves to the equal densities of the two components. For the small perturbations to the wave functions and considering the perturbations in plane wave form, we obtain the linearized Gross–Pitaevskii (GP) equations and the dispersion relation. In the nondissipative

* **Corresponding author: Haiming Deng,** School of Physics and Electronic-Electrical Engineering, Xiangnan University, Chenzhou 423000, China, e-mail: woshidenghaiming@126.com
Chao Kong, **Bin Yin**, **Jiaxin Wu**, **Jianquan Huang**, **Dajun Lei**, **Chunzhi Jiang:** School of Physics and Electronic-Electrical Engineering, Xiangnan University, Chenzhou 423000, China

regime, we focus on two special cases corresponding SOC strength $\alpha = 0$ and $\alpha \neq 0$. In the absence of SOC, we analytically present the dispersion relations of zero or nonzero helicoidal gauge potential cases and conclude the parameter conditions for MI occurrence. In the presence of SOC, we display the detailed analyses of the effects of the helicoidal gauge potential, SO-coupled strength, and nonlinear interactions on MI. The results indicate that (a) the MI gain ξ and the MI region in parameter plane (α, β) are symmetry about $\beta = 0$ or $\alpha = 0$; (b) the MI gain ξ increases gradually, and the regions of MI have changed from a complete one to two independent ones with the increase of wave number k. The larger values of MI gain ξ and the bigger MI region corresponding to the larger atomic interactions g and $|g_0|$ are also found. We clearly find that in parameter plane (k, α), the presence of helicoidal gauge potential β makes the effects of SOC on the MI more complex and more abundant MI regions appear. We also display that more abundant MI regions appears and the MI gain ξ of the system decreases gradually with the increase in SOC strength. In the dissipative regime, we investigate the effects of dissipative strengths on MI and find some interesting results. Our results provide a potential way to manipulate the MI in the helicoidal SO-coupled Bose–Bose mixtures. A natural direction is to extend the present analysis to two- or three-dimensional systems in order to explore more elaborated and composite structures.

2 Model and linear stability

Considering a uniform 1D Bose gas made of two species, in the weak-interaction limit, the corresponding energy density including the LHY corrections is

$$H_{1D} = \frac{g}{2}(|\Phi_1|^2 - |\Phi_2|^2)^2 + \frac{\delta g}{2}(|\Phi_1|^2 + |\Phi_2|^2)^2 - \frac{2g^{3/2}}{3\pi}(|\Phi_1|^2 + |\Phi_2|^2)^{3/2}, \tag{1}$$

where $\Phi_j (j = 1, 2)$ are the bosonic states, and we have considered the units $\hbar = m = 1$. The parameter δg is related to the coupling constants in the two spinor components as $\delta g = g + g_{12}$, with g and g_{12} being the intra- and inter-component interactions that can be experimentally adjusted independently [39,40]. Here, we have considered the repulse intra-component interaction, $g > 0$, and the attractive inter-component interaction, $g_{12} < 0$. The single-particle Hamiltonian H_0 of the system is given by:

$$H_0 = [p + \alpha A(x)]^2/2 + \Delta\sigma_z/2, \tag{2}$$

where $p = -i\partial/\partial x$, $A(x)$, Δ, and σ_z are, respectively, the momentum operator, spatially varying gauge potential with amplitude α, the Zeeman splitting, and Pauli matrices. A gauge transformation, $\Phi = e^{-i(\alpha^2+\beta^2)t/2}e^{-i\sigma_z\beta x}\Psi$, is adopted to switch to the rotating frame for the chosen gauge field $A(x)$ [41]. The dynamics of the Bose–Bose mixtures for different components is given by the nonlinear GP equations [38,42,43]:

$$\begin{aligned} i\frac{\partial\Psi_j}{\partial t} = &\left[-\frac{1}{2}\frac{\partial^2}{\partial x^2} + (-1)^{3-j}\frac{\Delta}{2} + \frac{\delta g}{2}(|\Psi_1|^2 + |\Psi_2|^2)\right. \\ &\left. - (-1)^j g(|\Psi_1|^2 - |\Psi_2|^2) - \frac{g^{3/2}}{\pi}(|\Psi_1|^2 + |\Psi_2|^2)^{\frac{1}{2}}\right]\Psi_j \\ &+ i\left[(-1)^{3-j}\beta\frac{\partial}{\partial x}\Psi_j - \alpha\frac{\partial}{\partial x}\Psi_{3-j}\right] \\ &+ i\left(\varepsilon - \kappa|\Psi_j|^2 + \gamma\frac{\partial^2}{\partial x^2}\right)\Psi_j, \end{aligned} \tag{3}$$

for $j = 1, 2$. Here, parameters β and α represent the helicoidal gauge potential and SOC, respectively. The SOC strength, of course, can be adjusted by the magnitude and direction of the Raman laser wave vector [21]. In one dimension, the beyond-mean-field terms are directly obtained from the second-order perturbation theory, and a positive mean-field imbalance is needed, $\delta g > 0$ [14]. Three dissipative terms are taken into account that are proportional to the positive constants ε, κ, and γ, respectively. The constant ε models the feeding strength from the thermal cloud, κ measures the losses due to two-body recombination, and γ denotes the losses that follow from the inhomogeneous dissipation process [44–46]. The total number of atoms are $\int(|\Psi_1|^2 + |\Psi_2|^2)\mathrm{d}x = N_1 + N_2 = N$.

In the framework of Eq. (3), the MI of the flat states with equal densities $n_1 = n_2 = n$ and the common chemical potential μ of both components: $\Psi_j = e^{-i\mu t}\sqrt{n}$. The densities, Zeeman splitting, interactions, and chemical potential are determined by the following algebraic equations:

$$\mu = \delta g n - \frac{g^{3/2}}{\pi}\sqrt{2n} + (-1)^{3-j}\frac{\Delta}{2} + i(\varepsilon - \kappa n). \tag{4}$$

For perturbed wave functions of the form $\Psi_j = e^{-i\mu t}(\sqrt{n} + \delta\psi_j)$, linearized equations for the small perturbations are as follows:

$$\begin{aligned} i\frac{\partial\delta\psi_j}{\partial t} = &-\frac{1}{2}\frac{\partial^2}{\partial x^2}\delta\psi_j + i\left[(-1)^{3-j}\beta\frac{\partial}{\partial x}\delta\psi_j - \alpha\frac{\partial}{\partial x}\delta\psi_{3-j}\right] \\ &+ n\left(\frac{\delta g}{2} + g\right)(\delta\psi_j + \delta\psi_j^*) + n\left(\frac{\delta g}{2} - g\right) \\ &\times(\delta\psi_{3-j} + \delta\psi_{3-j}^*) - \frac{g^{3/2}\sqrt{n}}{2\sqrt{2}\pi}(\delta\psi_j + \delta\psi_j^* + \delta\psi_{3-j} \\ &+ \delta\psi_{3-j}^*) + i\gamma\frac{\partial^2}{\partial x^2}\delta\psi_j - i\kappa n(\delta\psi_j + \delta\psi_j^*), \end{aligned} \tag{5}$$

where ψ^* stands for the complex conjugate of ψ. We consider the solutions of the perturbation as follows:

$$\delta\psi_j = \xi_j \cos(kx - \Omega t) + i\eta_j \sin(kx - \Omega t), \tag{6}$$

where k is the real wave number, Ω is the complex eigenfrequency, and ξ_j and η_j are amplitudes. By substituting Eq. (6) into Eq. (5), we have a set of linearly coupled equations for perturbation amplitudes ξ_j and η_j

$$M \times (\xi_1, \xi_2, \eta_1, \eta_2)^T = 0, \tag{7}$$

where M is a 4×4 matrix. Under condition with $\det M = 0$, the dispersion relation is obtained

$$\Omega^4 + P_2\Omega^2 + P_1\Omega + P_0 = 0, \tag{8}$$

where

$$\begin{aligned}
P_2 &= \frac{k^2}{2\pi}[g^{3/2}\sqrt{2n}(1 - 2i\gamma) + \pi(k^2(i + 2\gamma)^2 - 4(\alpha^2 + \beta^2) \\
&\quad + 2n(i + 2\gamma)(2ig + 2\kappa + i\delta g))], \\
P_1 &= \frac{k^3\alpha\sqrt{n}(1 - 2i\gamma)}{\pi}(\sqrt{2}g^{3/2} + 2\sqrt{n}\pi(2g - \delta g)), \\
P_0 &= \frac{k^4}{16\pi}[k^2(i + 2\gamma)^2 + 4(\alpha^2 + \beta^2 + n(i + 2\gamma)(2ig + \kappa))] \\
&\quad \times [2\sqrt{2n}g^{3/2}(1 - 2i\gamma) + \pi k^2(i + 2\gamma)^2 + 4\pi(\alpha^2 \\
&\quad + \beta^2 + n(i + 2\gamma)(\kappa + i\delta g))].
\end{aligned} \tag{9}$$

Solving Eqs. (8) and (9), we can obtain the results

$$\begin{aligned}
\Omega_{1,2} &= \frac{1}{2}\sqrt{\frac{-2P_2}{3} + \Lambda} \pm \frac{1}{2}\sqrt{\frac{-4P_2}{3} - \Lambda + \frac{2P_1}{\sqrt{-2P_2/3 + \Lambda}}}, \\
\Omega_{3,4} &= \frac{-1}{2}\sqrt{\frac{-2P_2}{3} + \Lambda} \\
&\quad \pm \frac{1}{2}\sqrt{\frac{-4P_2}{3} - \Lambda - \frac{2P_1}{\sqrt{-2P_2/3 + \Lambda}}},
\end{aligned} \tag{10}$$

with the parameters

$$\begin{aligned}
\Lambda &= \frac{\sqrt[3]{2}\Lambda_1}{3\sqrt[3]{\Lambda_2 + \sqrt{-4\Lambda_1^3 + \Lambda_2^2}}} + \frac{\sqrt[3]{\Lambda_2 + \sqrt{-4\Lambda_1^3 + \Lambda_2^2}}}{3\sqrt[3]{2}}, \\
\Lambda_1 &= P_2^2 + 12P_0, \\
\Lambda_2 &= 2P_2^3 + 27P_1^2 - 72P_0P_2.
\end{aligned} \tag{11}$$

Clearly, the value of Ω may be positive, negative, or complex, depending on the signs and magnitudes of the terms involved. The flat state is stable when Ω is real; otherwise, the MI growth rate (gain) is determined by the largest absolute value of the imaginary part of eigenfrequency:

$$\zeta = |\mathrm{Im}(\Omega)|_{\max}. \tag{12}$$

It is well known that, the Zeeman splitting Δ has not appeared in the dispersion relation for instability, which means that it cannot affect the properties of the MI. In the following research, we will focus on the effects of SOC, the helicoidal potential, dissipative strengths, and the atomic interactions on the MI.

3 MI without dissipative terms

3.1 MI in the absence of SOC

In the absence of SOC, we here focus on two special cases corresponding to $\beta = 0$ and $\beta \neq 0$.

Case 1. Zero helicoidal gauge potential. For $\beta = 0$, the model amounts to the usual two-component system with Rabi coupling, and our solution for Ω^2 is

$$\begin{aligned}
\Omega_+^2 &= \frac{k^2}{4}(k^2 + 8gn), \\
\Omega_-^2 &= \frac{k^2}{4\pi}(-2\sqrt{2n}g^{3/2} + k^2\pi + 4\pi n\delta g).
\end{aligned} \tag{13}$$

It is well known that, in this case, the Rabi coupling strength Δ has not appeared in the dispersion relation for instability and it means that it cannot affect the properties of the MI. Besides, for repulsive intracomponent and attract intercomponent interactions, Ω_+ is always real, and Ω_- is imaginary with $k^2 < \frac{2\sqrt{2n}g^{3/2}}{\pi} - 4n\delta g$, which is consistent with the results in the study by Bhuvaneswar et al. [37].

Case 2. Nonzero helicoidal gauge potential. In the presence of helicoidal gauge potential, Eqs. (8) and (9) are simplified as:

$$\Omega^4 + P_2\Omega^2 + P_0 = 0, \tag{14}$$

where

$$\begin{aligned}
P_2 &= \frac{k^2}{2\pi}g^{3/2}\sqrt{2n} - \pi[k^2 + 4(gn + \beta^2) + 2n\delta g], \\
P_0 &= \frac{k^4}{16\pi}[k^2 + 8gn - 4(\beta^2)]\{-2\sqrt{2n}g^{3/2} \\
&\quad + \pi[k^2 - 4(\beta^2 - n\delta g)]\}, \\
P_1 &= 0.
\end{aligned} \tag{15}$$

We have the dispersion relation

$$\Omega_\pm^2 = \frac{1}{2}(-P_2 \pm \sqrt{-4P_0 + P_2^2}). \tag{16}$$

Results show that stable configuration occurs for $\Omega_{\pm}^2 > 0$, whereas the MI takes place with complex $\Omega_{\pm}^2$. In the present scenario, the dispersion relation is complex in the following cases: (a) when $P_0 > P_2^2/4$, both $\Omega_{\pm}^2$ are complex; (b) when $0 < P_0 < P_2^2/4$ and $P_2 > 0$, both $\Omega_{\pm}^2$ are complex; and (c) irrespective of the value of P_2 but for $P_0 < 0$, Ω_{+}^2 is always positive, while Ω_{-}^2 is negative.

3.2 MI in the presence of SOC

To explore the effect of the SOC and the helicoidal gauge potential on MI, Figure 1 illustrates the MI gain ξ in the (α, β) plane with different wave numbers k when the atomic interactions g_0 and g satisfy the condition of $g + g_0 = 0.5$. Figure 1 shows that the MI takes place when α and β satisfy certain

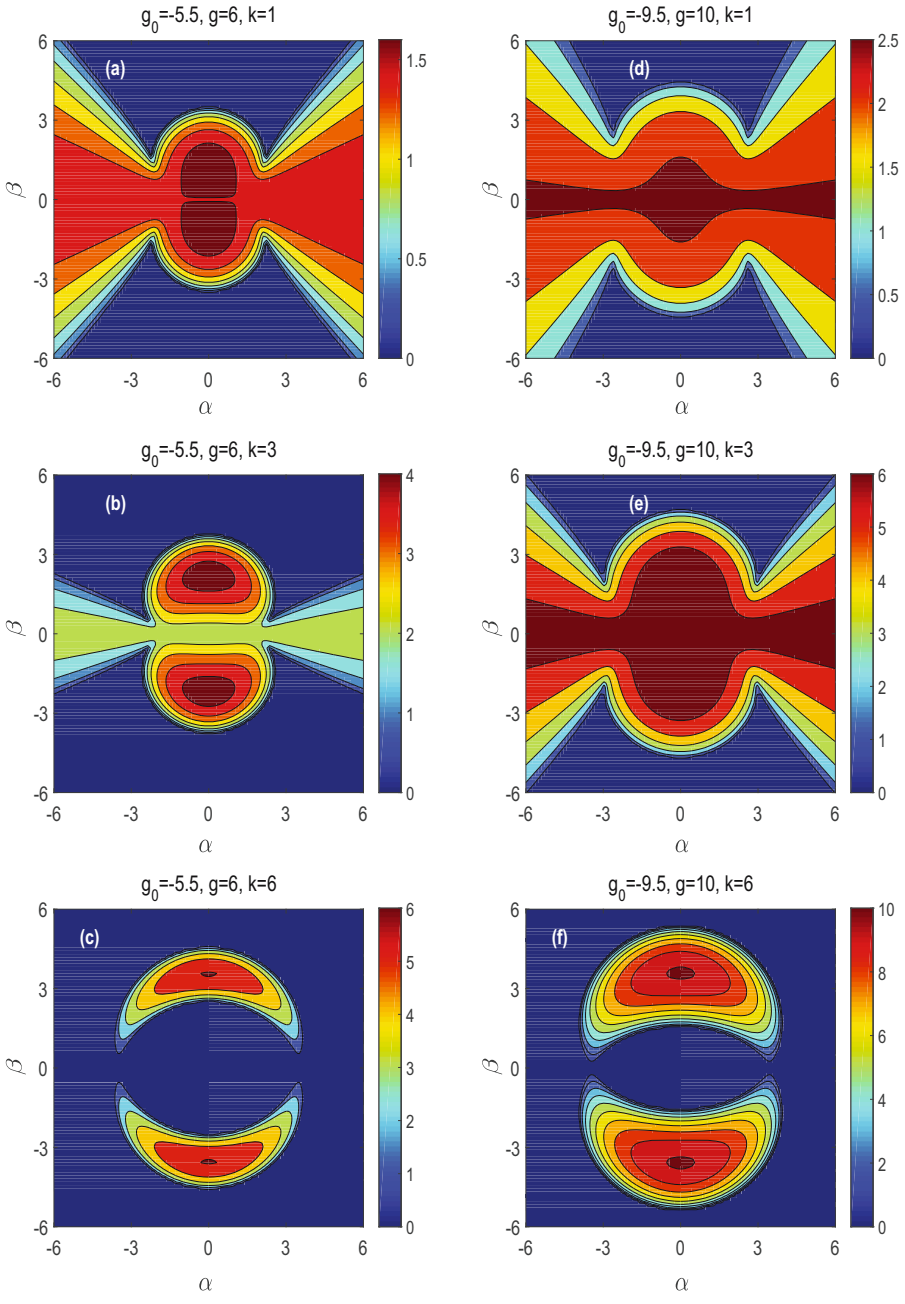

Figure 1: The contour plot of the MI gain ξ as a function of α and β for different atomic interactions and wave number. The first column: $k = 1$ in (a), 3 in (b) and 6 in (c). In this column, $g_0 = -5.5$ and $g = 6$ are fixed. The second column: $k = 1$ in (d), 3 in (e) and 6 in (f). In this column, $g_0 = -9.5$ and $g = 10$ are fixed.

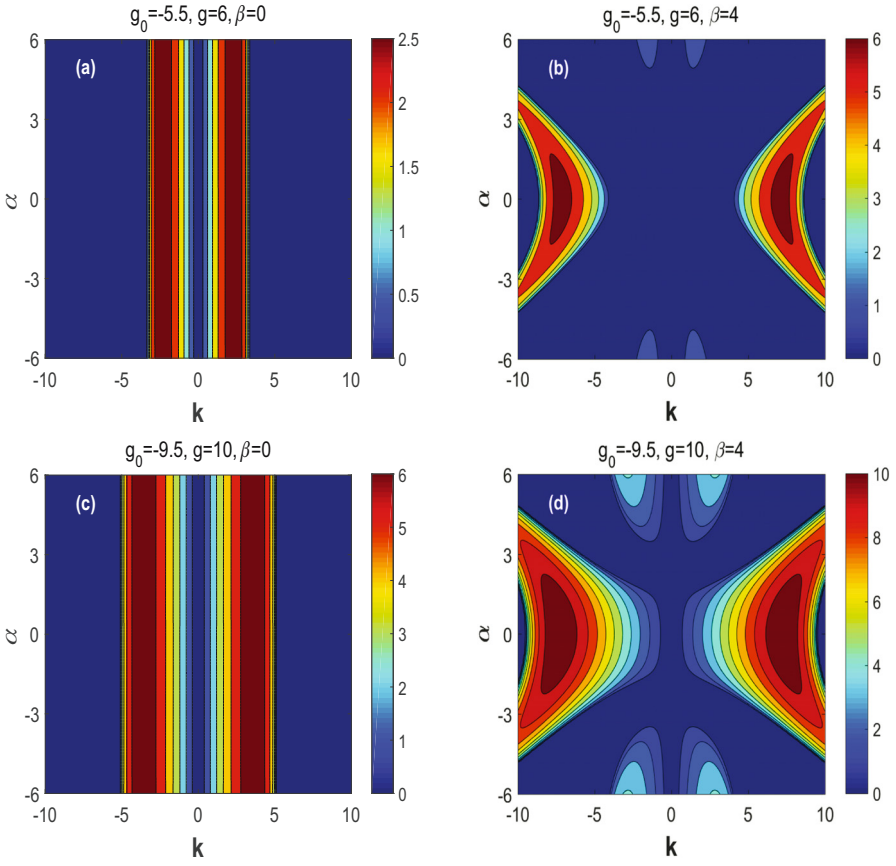

Figure 2: The contour plot of the MI gain ξ in the (k, α) with different atomic interactions and helicoidal gauge potential β. The first row: $\beta = 0$ in (a), and 4 in (b). In this row, $g_0 = -5.5$ and $g = 6$ are fixed. The second row: $\beta = 0$ in (c), and 4 in (d) where $g_0 = -9.5$ and $g = 10$ are fixed.

conditions. It is interesting to note that the MI gain ξ and the MI region for β (α) are symmetry about $\beta = 0$ ($\alpha = 0$). To interpret the symmetry of the MI regions in Figure 1, we make the following analysis. From the dispersion relation Eqs. (9) and (10), we can find that the helicoidal gauge potential β appears in the form of β^2, which leads to the symmetric region of the MI and the MI gain about $\beta = 0$. The symmetry of MI about α is described by the parameter P_1. Replacing the coefficient P_1 with $-P_1$ in Eq. (10), we obtain $\Omega_1' = -\Omega_3$, $\Omega_2' = -\Omega_4$, $\Omega_3' = -\Omega_2$, and $\Omega_4' = -\Omega_1$, which has not affected the MI gain ξ. In other words, because the condition $|P_1(-\alpha)| = |P_1(\alpha)|$ is satisfied, the regions of the MI are symmetric about $\alpha = 0$. We also find that the MI gain ξ increases gradually, and the regions of MI have changed from a complete one to two independent ones with the increase of wave number k for two different sets of atomic interactions $(g_0, g) = (-5.5, 6)$ and $(-9.5, 10)$. Besides, the system remains stable for larger wave number k when both $\alpha = 0$ and $\beta = 0$ are satisfied as shown in Figure 1(c) and (f). Under the condition of $\alpha = 0$ and $\beta = 0$, the dispersion relation Eq. (10) can be simplified to Eq. (13). For the fixed parameters g, g_0, and n, the larger wave number k satisfies $k^2 > \frac{2\sqrt{2n}g^{3/2}}{\pi} - 4n\delta g$, which leads to stable configuration; however, the MI takes place when $k^2 < \frac{2\sqrt{2n}g^{3/2}}{\pi} - 4n\delta g$ is satisfied. The larger values of atomic interactions g and $|g_0|$ corresponding to the larger MI gain ξ are also found.

In Figure 2, we plot the MI gain ξ in the plane of the (k, α) plane with different atomic interactions and helicoidal gauge potential β. For zero helicoidal gauge potential $\beta = 0$, the MI gain ξ in the (k, α) plane remains constant with the increase of α, as shown in Figure 2(a) and (c). Under conditions $\beta = 0$ and $\alpha \neq 0$, the dispersion relation Eq. (10) can be simplified to $\Omega_{1,2} = \frac{1}{2}(\pm k\sqrt{k^2 + 8gn} - 2k\alpha)$ and $\Omega_{3,4} = k\alpha \pm \frac{k}{2}\sqrt{k^2 - \frac{2\sqrt{2n}g^{3/2}}{\pi} + 4n\delta g}$, which means that the MI gain ξ is independent of SO-coupled strength α. From Figure 2(b) and (d), we clearly find that the presence of helicoidal gauge potential β makes the effects of SOC on the MI more complex and more abundant MI regions appear. Besides, the larger values of MI gain ξ corresponding to the larger atomic interactions g and $|g_0|$ are also found.

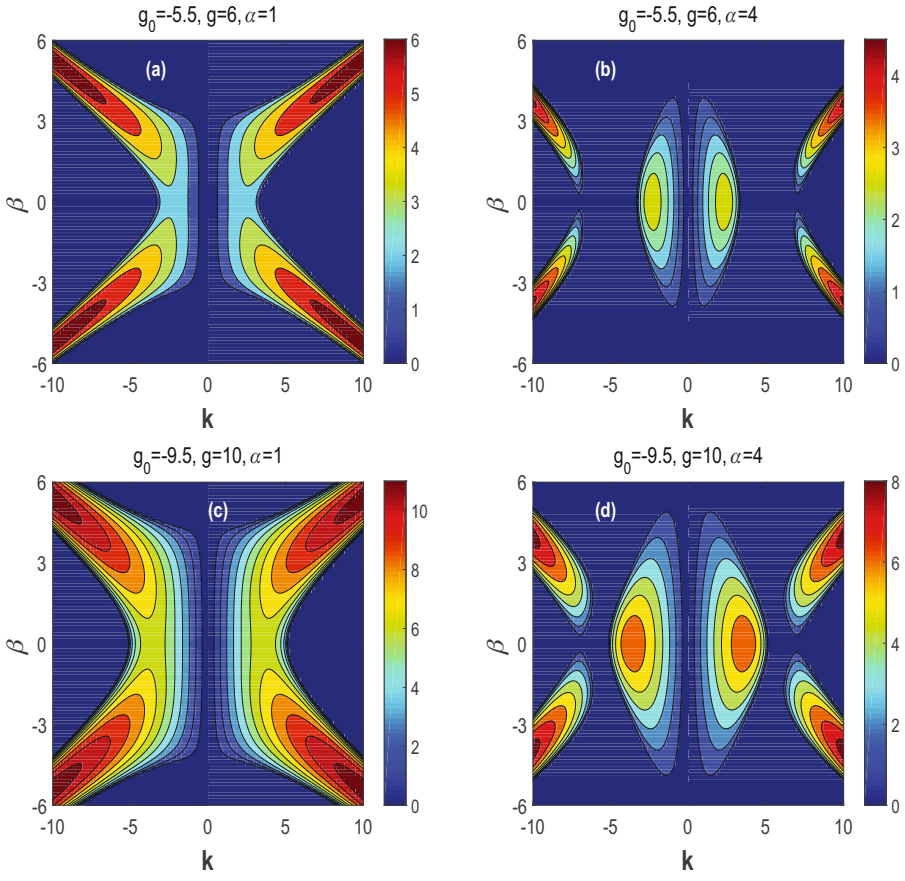

Figure 3: The contour plot of the MI gain ξ in the (k, β) with different atomic interactions and SOC α. The first row: $\alpha = 1$ in (a), and 4 in (b). In this row, $g_0 = -5.5$ and $g = 6$ are fixed. The second row: $\alpha = 1$ in (c), and 4 in (d) where $g_0 = -9.5$ and $g = 10$ are fixed.

In order to illustrate the effects of helicoidal gauge potential β on the MI, we will give some detailed analysis in Figure 3, where we plot the MI gain ξ in the plane of the (k, β) plane with different atomic interactions $g_0 = -5.5$, $g = 6$, and $g_0 = -9.5$, $g = 10$. As shown in Figure 3(a) and (c), there exist two MI regions for SO-coupled strength $\alpha = 1$ and the regions are symmetric about $\beta = 0$ and $k = 0$. The MI gain ξ increases gradually, and the MI region

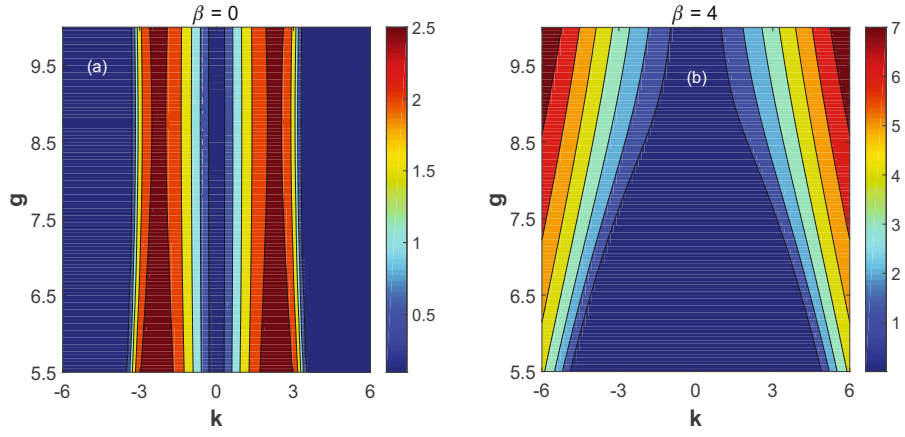

Figure 4: The contour plot of the MI gain ξ in the (k, g) with different helicoidal gauge potential (a) $\beta = 0$ and (b) $\beta = 4$. The other parameters are taken as $g_0 = 5.5$, $\alpha = 1$, $\kappa = 0.05$, and $\gamma = 0.01$.

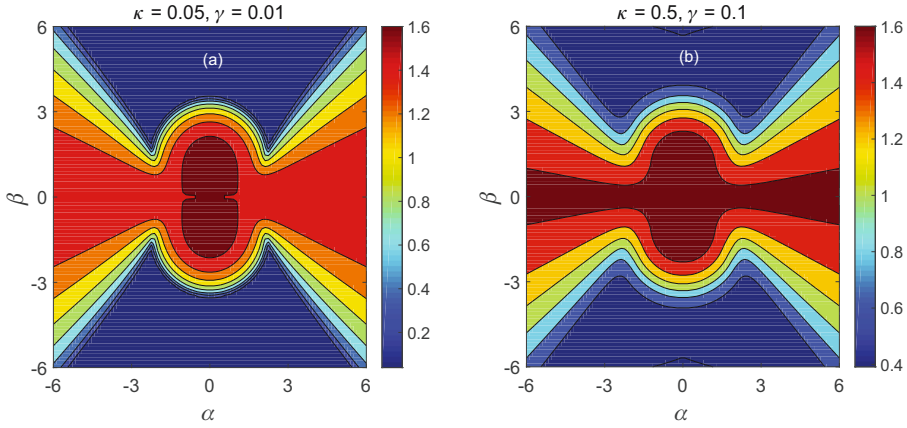

Figure 5: The contour plot of the MI gain ξ in the (α, β) with different dissipative strengths (a) $\kappa = 0.05$, $\gamma = 0.01$ and (b) $\kappa = 0.5$, $\gamma = 0.1$. The other parameters are taken as $g_0 = 5.5$, $g = 6$, and $k = 1$.

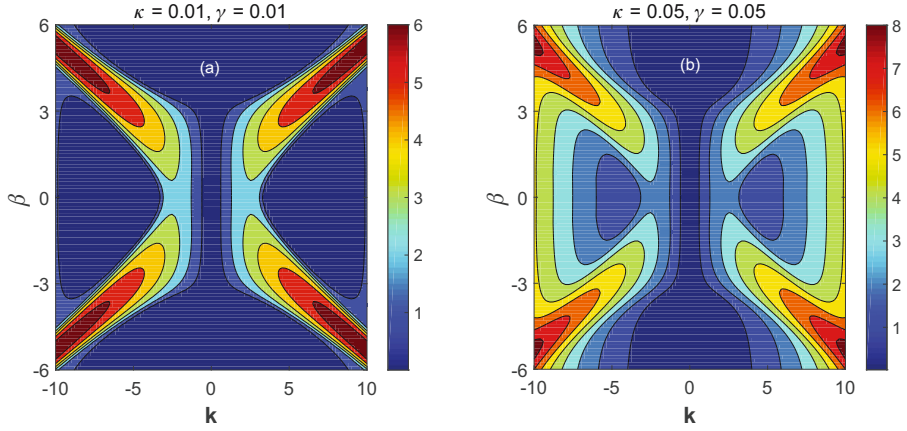

Figure 6: The contour plot of the MI gain ξ in the (k, β) with different dissipative strengths (a) $\kappa = 0.01$, $\gamma = 0.01$ and (b) $\kappa = 0.05$, $\gamma = 0.01$. The other parameters are taken as $g_0 = 5.5$, $g = 6$, $\alpha = 1$, and $k = 1$.

for k shrinks and shifts toward large $|k|$ region with the increase of $|\beta|$. The larger values of MI gain ξ and the bigger MI region corresponding to the larger atomic interactions g and $|g_0|$ are also found. By comparing Figure 3(a) and (c) with Figure 3(b) and (d), we find that the MI regions change from two to four and the MI gain ξ of the system decreases gradually with the increase in SOC strength.

4 MI with dissipative terms

In Figure 4(a), the MI gain ξ is plotted as a function of intra-atomic interaction and wave number for helicoidal gauge potential $\beta = 0$. The other parameters are taken as $g_0 = -5.5$, $\alpha = 1$, $\kappa = 0.05$, and $\gamma = 0.01$. It is observed that the MI region is symmetry about $k = 0$, which can be interpreted by the condition $|P_1(-k)| = |P_1(k)|$. For Figure 4(b) with helicoidal gauge potential $\beta = 4$, the larger values of MI gain ξ appears, and MI increases with increasing intra-atomic interaction. To explore the effect of dissipative strengths on MI, we plot the MI gain ξ in the (α, β) plane with different dissipative strengths: Figure 5(a) $\kappa = 0.05, \gamma = 0.01$, and Figure 5(b) $\kappa = 0.5, \gamma = 0.1$. Obviously, the instability zones with the maximum growth rate become larger with the increase of dissipation strengths. We also plot the MI gain ξ in the (k, β) in Figure 6 to illustrate the effects of dissipative for the labeled parameters. By comparing Figure 6(a) with Figure 6(b), we find that the larger values of MI gain ξ and more abundant MI regions appear for larger dissipative parameters.

5 Conclusion and discussion

In this article, we study the characteristics of MI of open Bose–Bose mixtures with helicoidal SOC by linear-stability

approach. For comprehensive research, we analyze the effects of the helicoidal gauge potential, SOC, different atomic interactions, and dissipative strengths on the MI and find some interesting results. Our analysis illustrates that for the nondissipative regime, the MI gain increases as wave number, helicoidal gauge potential, and the value of atomic interactions increase, while the opposite effect on MI gain occurs for SOC. Besides, more abundant MI regions appear for the larger SOC, wave number, helicoidal gauge potential, and the value of atomic interactions. In the dissipative regime, we also present the effects of dissipative strengths on MI. Our results present a feasible scheme to manipulate stability of helicoidal SO-coupled Bose–Bose mixtures.

A natural direction is to extend the present analysis to two- or three-dimensional systems in order to explore more elaborated and composite structures. It is well known that the solution of nonlinear equations is an important scientific problem. Under strongly nonlocal conditions, the nonlinear Schrödinger equation can also be simplified into a linear differential equation, and various soliton solutions and dynamic characteristics have been obtained [47–49], which are helpful to expand the method of solving nonlinear equations.

Funding information: This work was supported by the National Natural Science Foundation of China under Grant No. 11705155, Scientific Research Foundation of Xiangnan University for High-Level Talents, the Applied Characteristic Disciplines of Electronic Science and Technology of Xiangnan University (XNXY20221210), Innovation and Entrepreneurship Training Program for College Students in Xiangnan University ([2022]78), and Scientific Research Project of Xiangnan University ([2022]96).

Author contributions: All authors have accepted responsibility for the entire content of this manuscript and approved its submission.

Conflict of interest: The authors state no conflict of interest.

References

[1] Hasegawa A, Tappert F. Transmission of stationary nonlinear optical pulses in dispersive dielectric fibers. II. Normal dispersion. Appl Phys Lett. 1973;23:142.

[2] Ndzana F, Mohamadou A, Kofané TC. Modulational instability in a purely nonlinear coupled complex Ginzburg-Landau equations through a nonlinear discrete transmission line. Chaos 2008;18:043121.

[3] Kengne E, Lakhssassi A, Liu WM, Vaillancourt R. Phase engineering, modulational instability, and solitons of Gross-Pitaevskii-type equations in 1+1 dimensions. Phys Rev E 2013;87:022914.

[4] Megne LT, Tabi CB, Kofané TC. Modulation instability in nonlinear metamaterials modeled by a cubic-quintic complex Ginzburg-Landau equation beyond the slowly varying envelope approximation. Phys Rev E. 2020;102:042207.

[5] Tabi CB. Energy localization in an anharmonic twist-opening model of DNA dynamics. J Phys Condens Matter. 2010;22:414107.

[6] Maiiiina I, Tabi CB, EkobenaFouda HP, Mohamadou A, Kofané TC. Discrete impulses in ephaptically coupled nerve fibers. Chaos. 2015;25:043118.

[7] Tabi CB, Etémé AS, Mohamadou A, Kofané TC. Unstable discrete modes in Hindmarsh-Rose neural networks under magnetic flow effect. Chaos Solitons Fractals. 2019;123:116.

[8] Theocharis G, Rapti Z, Kevrekidis PG, Frantzeskakis DJ, Konotop VV. Modulational instability of Gross-Pitaevskii-type equations in 1+1 dimensions. Phys Rev A. 2003;67:063610.

[9] Salasnich L, Parola A, Reatto L. Modulational instability and complex dynamics of confined matter–wave solitons. Phys Rev Lett. 2003;91:080405.

[10] Kasamatsu K, Tsubota M. Multiple domain formation induced by modulation instability in two-component Bose–Einstein condensates. Phys Rev Lett. 2004;93:100402.

[11] Kasamatsu K, Tsubota M. Modulation instability and solitary-wave formation in two-component Bose–Einstein condensates. Phys Rev A. 2006;74:013617.

[12] Nguyen JHV, Luo D, Hulet RG. Formation of matter–wave soliton trains by modulational instability. Science. 2017;356:422–6.

[13] Petrov DS. Quantum mechanical stabilization of a collapsing Bose-Bose mixture. Phys Rev Lett. 2015;115:155302.

[14] Petrov DS, Astrakharchik GE. Ultradilute low-dimensional liquids. Phys Rev Lett. 2016;117:100401.

[15] Otajonov SR, Tsoy EN, Abdullaev FK. Modulational instability and quantum droplets in a two-dimensional Bose–Einstein condensate. Phys Rev A. 2022;106:033309.

[16] Kato YK, Myers RC, Gossard AC, Awschalom DD. Observation of the spin Hall effect in semiconductors. Science. 2004;306:1910–3.

[17] Konig M, Wiedmann S, Brü ne C, Roth A, Buhmann H, Molenkamp LW, et al. Quantum spin Hall insulator state in HgTe quantum wells. Science. 2007;318:766–70.

[18] Kane CL, Mele EJ. Topological Order and the Quantum Spin Hall Effect. Phys Rev Lett. 2005;95:146802.

[19] Bernevig BA, Hughes TL, Zhang SC. Quantum spin Hall effect and topological phase transition in HgTe quantum wells. Science. 2006;314:1757–61.

[20] Lin YJ, Jimenez-Garcia K, Spielman IB. Spin-orbit-coupled Bose–Einstein condensates. Nature. 2011;471:83–6.

[21] Jimenez-Garcia K, LeBlanc LJ, Williams RA, Beeler MC, Qu C, Gong M, et al. Tunable spin-orbit coupling via strong driving in ultracold-atom systems. Phys Rev Lett. 2015;114:125301; Salerno M, Abdullaev FK, Gammal A, Tomio L. Tunable spin–orbit-coupled Bose–Einstein condensates in deep optical lattices. Phys. Rev. A 2016;94:043602.

[22] Zhang YP, Mao L, Zhang CW. Mean-field dynamics of spin-orbit coupled Bose–Einstein condensates. Phys Rev Lett. 2012;108:035302.

[23] Hu FQ, Wang JJ, Yu ZF, Zhang AX, Xue JK. Collective dynamics of a spin-orbit-coupled Bose–Einstein condensate. Phys Rev E. 2016;93:022214.

[24] Kaur P, Gautam S, Adhikari SK. Supersolid-like solitons in a spin-orbit-coupled spin-2 condensate. Phys Rev A. 2022;105:023303.
[25] Luo HB, Malomed BA, Liu WM, Li L. Tunable energy-level inversion in spin-orbit-coupled Bose–Einstein condensates. Phys Rev A. 2022;106:063311.
[26] Roy A, Gautam S. Collective excitations in cigar-shaped spin-orbit-coupled spin-1 Bose–Einstein condensates. Phys Rev A. 2022;106:013304.
[27] Garcia-March MA, Mazzarella G, DellAnna L, Juliá-Diiiiaz B, Salasnich L, Polls A. Josephson physics of spin-orbit-coupled elongated Bose–Einstein condensates. Phys Rev A. 2014;89:063607.
[28] Luo X, Yang B, Cui J, Guo Y, Li L, Hu Q. Dynamics of spin-orbit-coupled cold atomic gases in a Floquet lattice with an impurity. J Phys B. 2019;52:085301.
[29] Luo X, Zeng ZY, Guo Y, Yang B, Xiao J, Li L, et al. Controlling directed atomic motion and second-order tunneling of a spin-orbit-coupled atom in optical lattices. Phys Rev A. 2021;103:043315; Luo X, Hu Z, Zeng ZY, Luo Y, Yang B, Xiao J, et al. Analytical results for the superflow of spin–orbit-coupled Bose–Einstein condensates in optical lattices. Phys Rev A. 2021;103:063324; Tang J, Hu Z, Zeng ZY, Xiao J, Li L, Chen Y, et al. Spin Josephson effects of spin–orbit-coupled Bose–Einstein condensates in a non-Hermitian double well. J Phys B. 2022;55:245301.
[30] Kong C, Luo X, Chen H, Luo Y, Hai W. Phase-controlled and chaos-assisted or-suppressed quantum entanglement for a spin-orbit coupled Bose–Einstein condensate. Chaos. 2019;29:103148.
[31] Bhuvaneswari S, Nithyanandan K, Muruganandam P, Porsezian K. Modulational instability in one-dimensional spin-orbit coupled quantum droplets. J Phys B. 2016;49:245301.
[32] Mithun T, Kasamatsu K. Modulation instability associated nonlinear dynamics of spin-orbit coupled Bose–Einstein condensates. J Phys B. 2019;52:045301.
[33] Bhat IA, Mithun T, Malomed BA, Porsezian K. Modulational instability in binary spin-orbit-coupled Bose–Einstein condensates. Phys Rev A. 2015;92:063606.
[34] Tabi CB, Otlaadisa P, Kofané TC. Modulation instability of two-dimensional Bose–Einstein condensates with helicoidal and a mixture of Rashba-Dresselhaus spin-orbit couplings. Phys Lett A. 2022;449:128334.
[35] Li XX, Cheng RJ, Zhang AX, Xue JK. Modulational instability of Bose–Einstein condensates with helicoidal spin-orbit coupling. Phys Rev E. 2019;100:032220.
[36] Rechtsman MC, Zeuner JM, Plotnik Y, Lumer Y, Podolsky D, Dreisow F, et al. Photonic Floquet topological insulators. Nature (London). 2013;496:196–200.
[37] Singh D, Parit MK, Raju TS, Panigrahi PK. Modulational instability in a one-dimensional spin-orbit coupled Bose-Bose mixture. J Phys B. 2020;53:245001.
[38] Tabi CB, Veni S, Kofané TC. Generation of matter waves in Bose-Bose mixtures with helicoidal spin-orbit coupling. Phys Rev A. 2021;104:033325.
[39] Blatt S, Nicholson TL, Bloom BJ, Williams JR, Thomsen JW, Julienne PS, et al. Measurement of optical Feshbach resonances in an ideal gas. Phys Rev Lett. 2011;107:073202.
[40] Inouye S, Andrews MR, Stengeretal J. Observation of Feshbach resonances in a Bose–Einstein condensate. Nature (London). 1998;392:151.
[41] Y.V. Kartashov, V.V. Konotop. Solitons in Bose–Einstein condensates with helicoidal spin-orbit coupling. Phys Rev Lett. 2017;118:190401.
[42] Tononi A, Wang YM, Salasnich L. Quantum solitons in spin-orbit-coupled Bose-Bose mixtures. Phys Rev A. 2019;99:063618.
[43] Otlaadisa P, Tabi CB, Kofané TC. Modulation instability in helicoidal spin-orbit coupled open Bose–Einstein condensates. Phys Rev E. 2021;103:052206.
[44] Luo X, Hai W. Dynamic chaos and stability of a weakly open Bose–Einstein condensate in a double-well trap. Chaos. 2005;15:033702.
[45] Coullet P, Vandenberghe N. Chaotic dynamics of a Bose–Einstein condensate in a double-well trap. J Phys B. 2002;35:1593; Chaotic self-trapping of a weakly irreversible double Bose condensate. Phys Rev E. 2001;64:025202(R).
[46] VictoFilho S, Abdullaev FK, Gammal A, Tomio L. Autosolitons in trapped Bose–Einstein condensates with two-and three-body inelastic processes. Phys Rev A. 2001;63:053603.
[47] Shen S, Yang Z, Pang ZG, Ge YR. The complex-valued astigmatic cosine-Gaussian soliton solution of the nonlocal nonlinear Schrödinger equation and its transmission characteristics. Appl Math Lett. 2022;125:107755.
[48] Song LM, Yang ZJ, Li XL, Zhang SM. Coherent superposition propagation of Laguerre-Gaussian and Hermite-Gaussian solitons. Appl Math Lett. 2020;102:106114.
[49] Shen S, Yang Z, Li X, Zhang S. Periodic propagation of complex-valued hyperbolic-cosine-Gaussian solitons and breathers with complicated light field structure in strongly nonlocal nonlinear media. Comm Nonlinear Sci Numer Simul. 2021;103:106005.